A new technique for obtaining time-of-flight signals in a one dimensional polymer single crystal

1992 J. Phys.: Condens. Matter 4 2543

(http://iopscience.iop.org/0953-8984/4/10/017)

J. Phys.: Condens. Matter 4 (1992) 2543–2555. Printed in the UK

A new technique for obtaining time-of-flight signals in a one-dimensional polymer single crystal

N E Fisher

Department of Physics, King's College London, Strand, London WC2R 2LS, UK

Received 22 November 1991

Abstract. This paper presents a new technique for observing carrier motion in the polymer bis(*p*-toluene sulphonate) ester of 2,4-hexadiyne-1,6-diol (PDATS). Using a three-electrode system, time-of-flight signals can be observed under low carrier density, bipolar conditions. A direct determination of carrier drift velocity can thus be obtained. Qualitative explanations for the action of this technique are given and comparisons are made of the results found using this technique with those found using surface configuration Kepler/LeBlanc time-of-flight experiments.

1. Introduction

The polymer bis(*p*-toluene sulphonate) ester of 2,4-hexadiyne-1,6-diol (PDATS) is easily produced as millimetre-sized single crystals in which the polymer backbone direction is well defined and common to all chains in the sample [1]. Because the chain separation is large (0.7 nm) compared to the repeat unit distance on a chain (0.45 nm) [2], each may be considered as an independent, quasi-one-dimensional semiconductor. Dark conductivity measurements along and perpendicular to the chains by Siddiqui and Wilson [3] show an anisotropy of over 1000 reflecting this one-dimensional nature. Experiments on PDATS may then, offer an insight into one-dimensional carrier motion.

Controversy however, concerning the motion of photogenerated carriers along the chains does exist. For instance, Donovan and Wilson in their photoconductivity experiments [4], interpret their results as showing carrier drift that is electric-field saturated at acoustic velocities down to the smallest fields (10^2 V m^{-1}) at which their measurements prove possible. This they attribute to the charge-carrier mechanism as that of the solitary wave acoustic polaron (SWAP) where current carriers are formed from the interaction of electrons (or holes) and the acoustic phonon field [5]. An ultra-high low field mobility in excess of 20 m^2 s^{-1} V^{-1} is deduced. In addition, they claim an inter-trap separation of the order 1 mm [6]. On the other hand, Heeger *et al* [7,8] report a carrier drift velocity that is linearly proportional to the applied field, while Blum and Bassler [9] deduce a carrier drift velocity that is weakly field dependent at low field ($< 5\times10^5$ V m^{-1}) and increases linearly proportionally to the applied field at higher electric field. These two groups also report carrier motion that is trap-limited, with inter-trap separations less than microns apart and observed trap-limited mobilities at least 10000 times less than that deduced by Donovan and Wilson [4,5].

0953-8984/92/102543+13$04.50

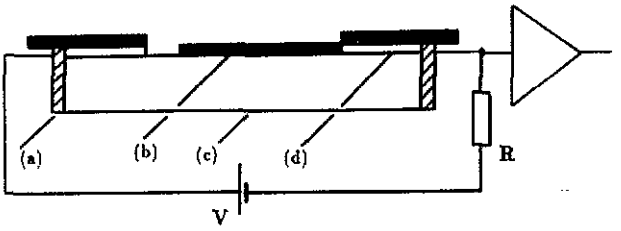

Figure 1. Arrangement (side-view) of surface-configuration transit current experiments: (*a*) silver paste, (*b*) optical mask with slit, (*c*) PDATS crystal, (*d*) evaporated Ag electrodes. Following a laser pulse, carriers are generated at the slit. Depending on the polarity of V, one sign of carrier traverses the sample, to induce a transit signal, while the other sign discharges almost immediately at its nearest electrode.

This controversy arises mostly because of the apparent ambiguity in interpreting photocurrents. (Typical current profiles and the experimental arrangement for obtaining them are shown in figure 9, see later.) For instance, from the analysis of transient photocurrent decays, Donovan and Wilson deduce macroscopic inter-trap distances while Blum and Bassler, using exactly the same experimental techniques, find microscopic inter-trap distances. In addition, Heeger *et al* observe a narrowing of current profile with applied field on sample lengths of the order 10–25 μm, which in their opinion reflects field-dependent trap-limited transport within this length, while Donovan and Wilson [10, 11] claim that what is actually being observed in these experiments are changes in profile due to faster bimolecular recombination rates because of increased carrier concentrations.

Recently, Fisher and Willock [12, 13], using a surface variation of the classic Kepler/LeBlanc [14, 15] time-of-flight experimental arrangement, (which will henceforth be referred to as the optical mask method and is illustrated in figure 1), find trap-limited transit currents for electrons only and inter-trap separations much less than 50 μm. Deduced drift velocities are are found to tend towards saturation at acoustic velocities with high field. Trap-limited mobilities are in agreement with the latter two groups. In addition, because of the absence of time-of-flight signals for holes (only a featureless decay is seen), the electrons are considered to be the dominant current carriers.

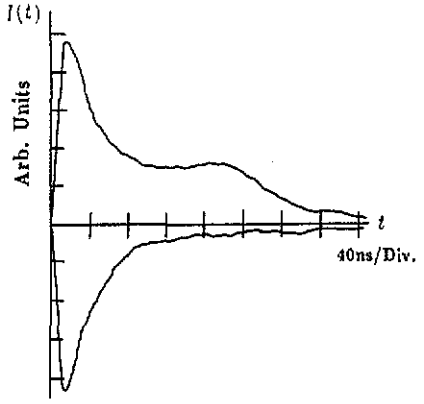

Figure 2. Transit signals obtained using the arrangement of figure 1 on a sample with electrode spacing 300 μm and an applied field of 2.47×10^6 V m^{-1}. The upper trace is obtained using a negative applied voltage. The lower trace is obtained using a positive applied voltage.

However, these experiments too appear open to interpretation: Donovan and Wilson ascribe the prolific trapping and trap-release events, which seem to constitute these unipolar time-of-flight signals, an example of which is shown in figure 2 along with its corresponding hole 'transit', to consequences of Coulomb effects between the relatively high density of carriers of the same sign traversing a one-dimensional system [16,17]. That is, in their opinion, a negative carrier on one chain when trapped in an hypothesized neutral trap can, because of its Coulomb radius, block the passage of negative carriers on neighbouring chains behind it, because they are constrained to drift along those chains, and cannot drift laterally as in three-dimensional systems. Those carriers that are far enough away from the trapped electron will, however, eventually be thermally activated and thus continue their drift. Therefore, what Donovan and Wilson consider is observed in these time-of-flight experiments are the continuous block and escape of carriers caused by a few intrinsically trapped electrons and not, as interpreted by the authors, prolific trapping and trap-release events caused by numerous traps intrinsic to the sample. The true trap density, according to them, can only be deduced when performing low-density bipolar current measurements, as in their own experiments, in which these hypothesized Coulomb effects are small.

As the transit signals are apparently open to interpretation, a three-electrode system was devised that allows time-of-flight signals to be observed under these low-density, bipolar conditions.

The experimental method and operation will first be discussed and the results and conclusions found using this technique compared with those found using the optical mask technique.

2. Experimental method and operation

The three-electrode system (henceforth referred to as the electron arrival detector—EAD) is shown in figure 3. A potential V, $V(D - L)D$ and zero is applied to electrodes 1,2 and 3 respectively. Electrodes 1 and 3 are silver electrodes evaporated onto the (100) face, and electrode 2 is a very thin (< 20 μm diameter) insulated wire laid on top of the (100) face. Following a laser pulse of duration 10 ns and photon energy 3.68 eV, electron–hole pairs are generated on the (100) face, in a skin depth

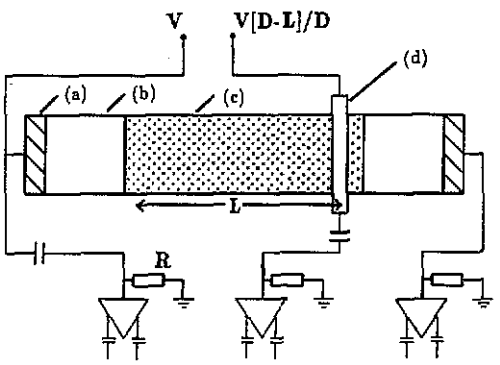

Figure 3. Arrangement (top-view) of EAD: (*a*) silver paste, (*b*) evaporated Ag electrode, (*c*) PDATS crystal, (*d*) thin insulated wire laid on top of the (100) face. D is the surface electrode spacing and L is the spacing between the wire and the left electrode.

of about 0.5 μm. As the carriers drift along the polymer chains, under the action of the applied electric fields (F-fields), they induce currents on the electrodes which are observed using amplifiers and a fast oscilloscope (Tektronix 7A26) having an overall response time of less than 10 ns. As will become clear, it is the signals on electrode 3, because they are time of flight, that will be of main interest. All experiments are performed with the samples under a vacuum of 10^{-6} Torr and at room temperature.

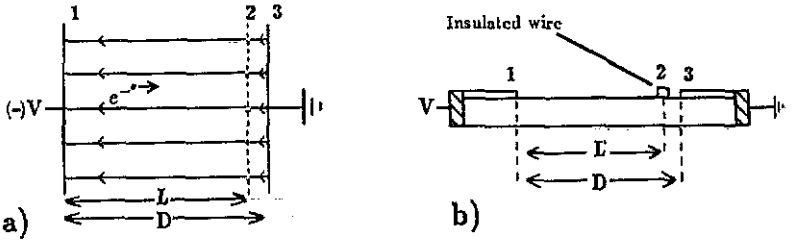

Figure 4. (*a*) EAD: idealized parallel plate geometry. Electrode 2 is a grid which allows an electron to drift through it. (*b*) EAD: side-view of surface configuration arrangement used in experiment.

Before describing the action of the EAD, it may be worth considering the three-electrode parallel plate arrangement of figure 4(*a*). Between plates 1 and 3, there is a grid that allows an electron (say) to pass from the region between 1 and 2, R12, to that between 2 and 3, R23. The electrodes 1,2 and 3 are held at potentials V, $V(D-L)D$, and zero respectively, where D is the distance between plates 1 and 3, and L is the distance between plates 1 and 2. The potential $V(D-L)D$ is applied to the grid to minimize its effect in disturbing the applied field between the two plates. In this ideal system then, the lines of F-field from 1 all end on 2, and then from 2 all end on 3.

An electron moving in the region R12 induces a charge on electrodes 1 and 2, but because it is outside the field lines of R23, no charge is induced on 3. It is only when the electron enters R23, through the grid, that a charge will be induced on it. In effect, the grid shields electrode 3 from any current induced by a charge which is drifting in R12.

Considering the surface electrode geometry of the EAD shown in figure 4(*b*), and adopting the same notation as above, if the majority of F-field lines near the sample surface from electrode 1 end on the wire (electrode 2), and then those from 2 end on 3, then for similar reasons the wire shields currents induced by a charge drifting near the surface in the region R12 from 3. Again, it is only when the carriers enter R23 that any currents will be induced on 3. It is this shielding effect by the wire that is responsible for the time of flight signals to be observed on electrode 3.

Using this proposed shielding idea, figure 5 shows the operation of the EAD under ideal conditions; an initial uniform density of negative carriers generated on the surface of the crystal which then drifts from left to right, with no diffusion or dispersion. The drift of holes in the opposite direction is, for the moment, not considered. Shown on the right are the currents, $I(t)$, induced on electrode 3. Carriers from R12 enter R23. With the rate of discharge of charge at 3 equal to the rate of charge entering R23, $I(t)$ maintains a constant value with respect to time. It is when no more charge enters R23 (figure 5(*c*)), that discharge starts to dominate. This is reflected by the sudden decrease of $I(t)$. It is this decrease at time t_τ that

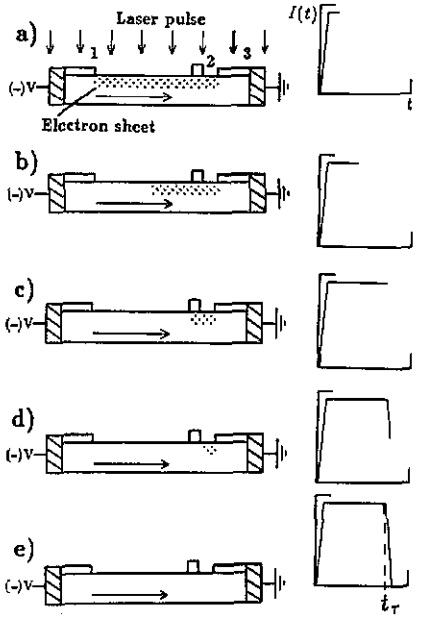

Figure 5. Idealized operation of the EAD. Following a laser pulse, a sheet of carriers is generated on the (100) face. The currents induced on electrode 3, due to their drift, are shown on the right.

tells us how long it has taken the carriers to traverse the distance L from electrode 1, to under the wire. A drift velocity may then be deduced using L/t_τ for a given applied field $F = V/D$. In experiment, any dispersion would tend to smear out this idealized transit signal.

By reversing the polarity of V, so that the electrons are made to drift from right to left and treating them as the dominant current carriers, the currents induced on 3 would then be expected to resemble a featureless decay, reflecting the loss of charge from R23 into R12.

3. Results

3.1. Wire position variation

With reference to figure 4(*b*), and using a sample with inter-electrode spacing D = 280 μm, this section looks at the currents induced on the wire and the surface electrodes when the wire is positioned at; (i) about 30 μm to the left of electrode 3 with a potential $V(D - L)D$ applied to it, (ii) about the centre of the sample with a potential $V/2$ applied to it, and (iii) about 30 μm to the right of electrode 1 with a potential $V(L/D)$ applied to it. Both polarities of the applied voltage are used.

Figures 6(*a*), (*b*) and (*c*) show the induced currents when the wire is at position (i) for negative V. With the electrons made to drift from left to right, a time-of-flight signal is observed on electrode 3. For this to occur, charge must be entering R23 from R12 as shown by the current reversal induced on the wire, which indicates that charge is drifting under it. As would be expected, the current on 1 is a featureless decay since only a small amount of charge is entering R12 from R23. When the polarity is reversed as in figures 6(*d*), (*e*) and (*f*), the signal on the wire shows no obvious current reversal, indicating that negligable positive charge is entering R23

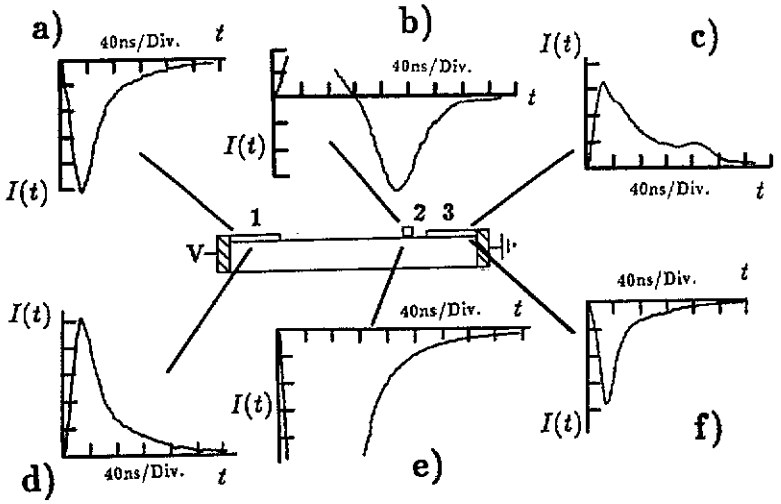

Figure 6. Induced currents on electrodes with wire at position (i). (*a*), (*b*) and (*c*) are for a negative applied voltage and (*d*), (*e*) and (*f*) are for a positive applied voltage. In both cases the applied field (V/D) is 2.86×10^6 V m^{-1} and the laser intensity is about 1.0×10^4 W m^{-2}. $I(t)$ for (*a*), (*c*), (*d*) and (*f*) each have the same arbitary units while $I(t)$ for (*b*) and (*e*) each have arbitary units that are about a factor 5 smaller.

from R12 (at the times looked at) and so, no transit signal is observed on 3. It would seem, therefore, that, as deduced using the optical mask method, the electrons are the dominant current carriers and, therefore, the signals induced on the electrodes are mainly dominated by their drift. Consequently, the signal on the wire is due mostly to that of the electrons in R12 drifting to the left with no current reversal observed, because the centre of charge of the sheet of electrons generated between 1 and 3 is always drifting away from (to the left of) the wire. Finally, with only a small amount of negative charge entering R12 from R23, the signal induced on 1 is dominated by the drift of carriers between 1 and 2, and so is featureless.

Figures 7(*a*), (*b*) and (*c*), show the induced currents when the wire is at position (ii) for negative V. With the electrons made to drift from left to right, a transit signal is observed on electrode 3 and a featureless decay on 1, in accord with the arguments given above. However, with the wire positioned at exactly $D/2$, the signal induced on it would be expected to exhibit no current reversal because the centre of charge of the negative sheet of carriers generated between 1 and 3, is always drifting away from (to the right of) the wire. However, a small reveral is observed, probably because the wire is positioned a little to the right of dead centre. With the polarity of V reversed, as in figures 7(*d*), (*e*) and (*f*), the transit signal is now observed on 1, and the featureless decay on 3. No current reversal is induced on the wire, as expected.

Finally, with the wire at position (iii), and the electrons drifting from left to right as in figures 8(*a*), (*b*) and (*c*), the induced currents, as expected, resemble those of figures 6(*f*), (*e*) and (*d*) respectively. Similarly, when made to drift to the left as in figures 8(*d*), (*e*) and (*f*), the currents resemble those of figures 6(*c*), (*b*) and (*a*) respectively.

These results, at least qualitatively, are consistant not only with the proposed operation of the EAD, but also with the premise that the negative carriers are the dominant current carriers.

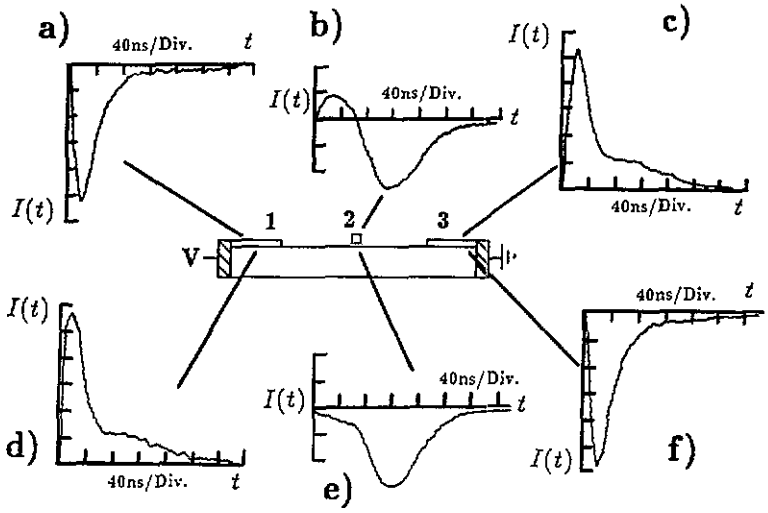

Figure 7. Induced currents on electrodes with wire at position (ii). (*a*), (*b*) and (*c*) are for a negative applied voltage and (*d*), (*e*) and (*f*) are for a positive applied voltage. The applied field, the laser intensity and the $I(t)$ scales, are as in figure 6.

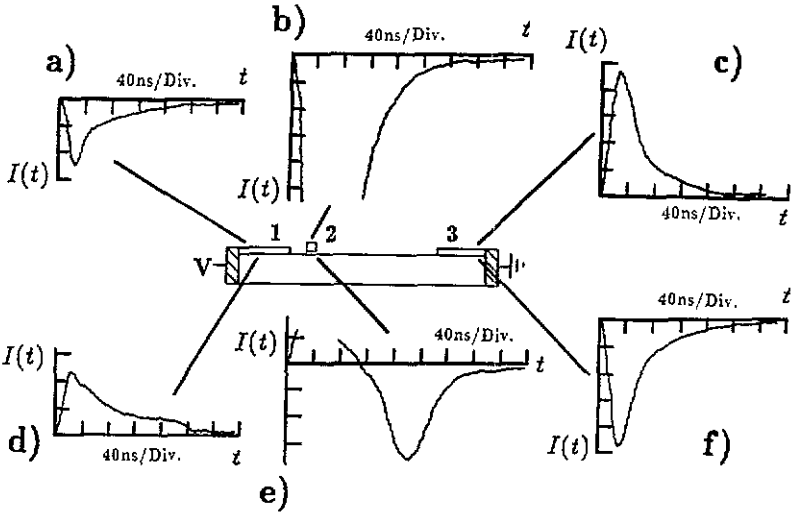

Figure 8. Induced currents on electrodes with wire at position (iii). (*a*), (*b*) and (*c*) are for a negative applied voltage and (*d*), (*e*) and (*f*) are for a positive applied voltage. The applied field, the laser intensity and the $I(t)$ scales, are as in figure 6.

3.2. Conservation of current

In a conventional two-electrode photoconductivity experiment, a general result is that the current $I(t)$ induced on the electrodes due to a sample charge q drifting a distance x, is given by

$$I(t) = (q/V)\frac{\delta V(x)}{\delta t} \tag{1}$$

where V is the potential between the plates, and $\delta V(x)$ is the potential change

through which the charge drifts in a time δt. It would be expected, therefore, that because the charge samples equal but opposite $\delta V(x)$s as it drifts with respect to each electrode, the induced currents on those electrodes will also be equal but opposite. Using the 10 ns laser pulse, and the experimental arrangement of figure 3 (but without the wire present) on a sample of electrode spacing about 260 μm, figure 9 shows this to be the case.

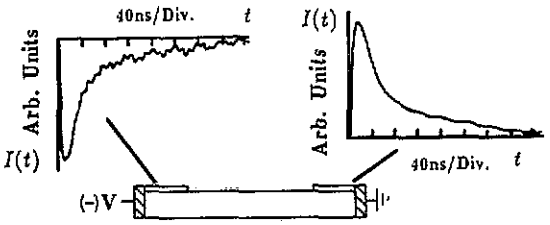

Figure 9. Induced currents using a conventional two-electrode system for a negative applied voltage. The applied field is 9.40×10^5 V m^{-1} and the laser intensity is about 1.0×10^5 W m^{-2}.

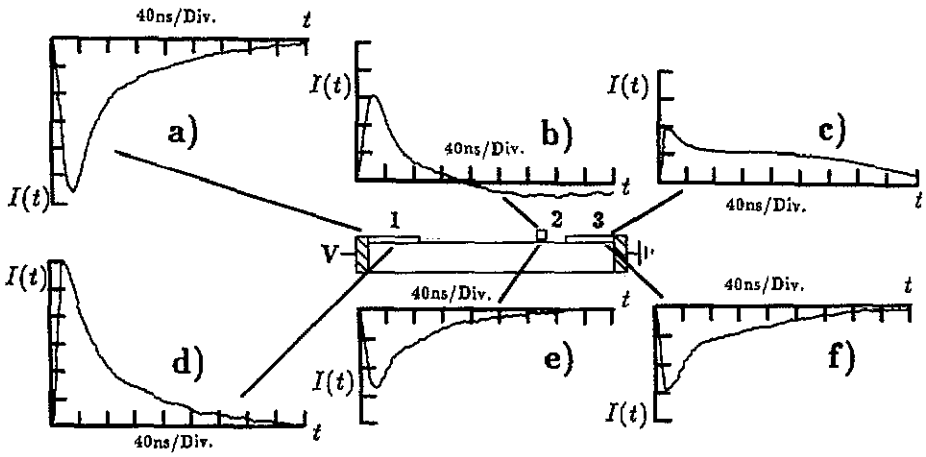

Figure 10. Induced currents on electrodes for a negative applied voltage [(*a*), (*b*) and (*c*)] and for a positive applied voltage [(*d*), (*e*) and (*f*)]. In both cases the applied field is 9.61×10^5 V m^{-1} and the laser intensity is about 1.0×10^5 W m^{-2}. $I(t)$ for all currents have the same arbitary units for comparison.

For the EAD, the wire may be considered to divide the sample surface into two two-electrode systems. Similar arguments to those above would again lead to current conservation where now the sum of the currents induced on all three electrodes is equal to zero. Using the same sample, but with the wire positioned about 30 μm to the left of the right electrode, figures 10 and 11 show these induced currents using both polarities of V, for two applied fields. As expected, current is conserved.

3.3. Field dependence and length dependence of time-of-flight signals

For the following results, the wire is again positioned about 30 μm to the left of the right electrode. It is the signals induced on this electrode following the 10 ns laser pulse which are now to be described.

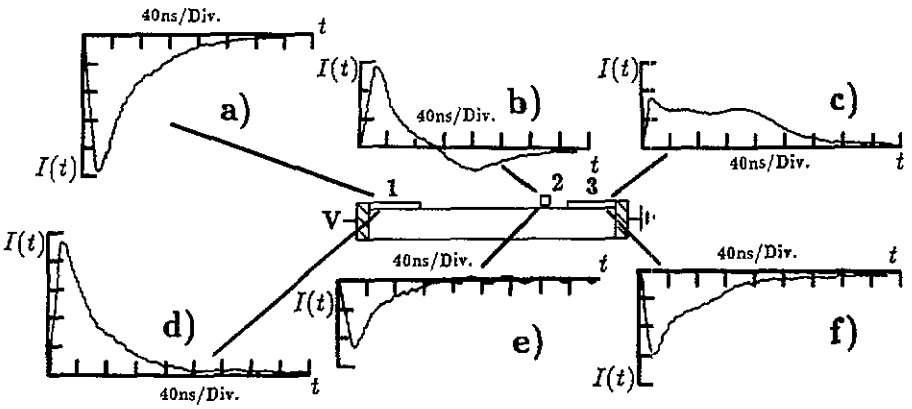

Figure 11. Induced currents on electrodes for a negative applied voltage [(*a*), (*b*) and (*c*)] and for a positive applied voltage [(*d*), (*e*) and (*f*)]. In both cases the applied field is 1.92×10^6 V m^{-1} and the laser intensity is about 3.3×10^4 W m^{-2}. $I(t)$ for all currents have the same arbitary units for comparison.

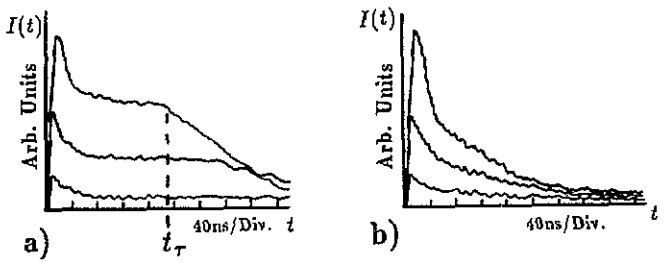

Figure 12. (*a*) Field dependence of current profiles induced on electrode 3 for negative applied voltages. Applied fields are 1.15×10^6 V m^{-1}, 7.69×10^5 V m^{-1} and 3.85×10^5 V m^{-1}. In all cases the laser intensity is about 1.0×10^5 W m^{-2}. (*b*) Field dependence of current profiles induced on electrode 3 for positive applied voltages. Applied fields and laser intensity are as in figure 12(*a*).

Typical current profiles at three fields (with the sheet of electons drifting from left to right) using a sample of inter-electrode spacing 260 μm, are shown in figure 12(*a*). Not only is the transition region field dependent, but also these signals exibit more dispersive profiles as the field is decreased. (This is also clear from figures 10(*c*) and 11(*c*).) In fact, it was generally found that at fields of less than about 5×10^5 V m^{-1}, the transition region is no longer visible and only a featureless decay is observed. Very similar changes in current profile were observed using the optical-mask experiments and suggest the presence of relatively shallow traps impeding the hypothesized intrinsic field-saturated SWAP drift. (We concentrate on Coulomb traps as opposed to barriers, since temperature-dependence experiments of the transit signals obtained using the optical mask technique exhibited activated behaviour [13].) With this the case, and this will be discussed further, the trap-release times of these traps must be field dependent and, for the faster carriers, less than the characteristic time (t_τ) of the experiment. Thus, at high fields the trap-release times are small implying that the carrier sheet (specifically its left edge) undergoes relatively little dispersion as it traverses the sample length. This leads to the sharply defined time-of-flight signals. At low fields, trap-release times are longer implying a greater range of release times,

which then tends to smear the carrier sheet and thus give rise to the more ill-defined transition regions.

Figure 12(*b*) shows the corresponding hole 'transits' (i.e. with the electrons drifting from right to left) and, as expected, no time-of-flight signals are observed.

Also shown in figure 12(*a*) for one of the time-of-flight signals, is the transit time t_τ which, as may be seen, is found by estimating the onset of the sharp decay at the transition region. Thus, by using the relations

$$v_d = L/t_\tau \tag{2}$$

$$\mu = v_d/F \tag{3}$$

where here $L = D - 30$ μm, the field dependence of the drift velocity (v_d) for the negative carriers may be plotted and their observed mobilities (μ) deduced. Using three samples cut from the same crystal but each with a different inter-electrode separation, figure 13 shows such a plot. As was also found using the optical-mask technique, at low fields the drift velocity is approximately linear with field, but at the higher fields the velocity tends toward saturation at acoustic velocities.

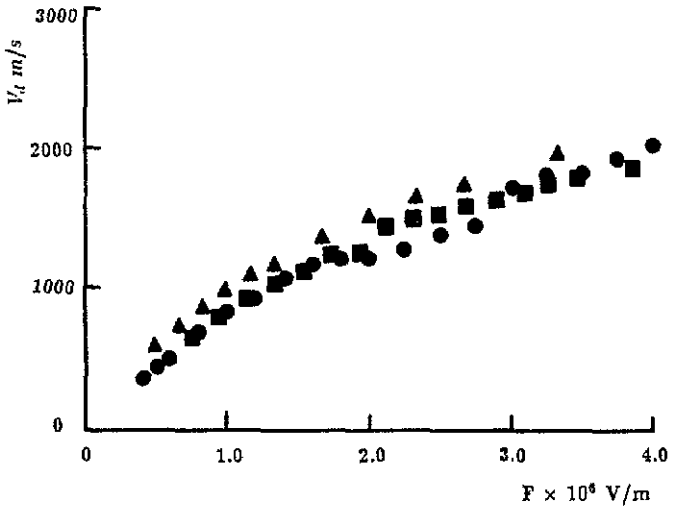

Figure 13. Field dependence of drift velocity for various samples: squares, L = 490 μm; triangles, L = 270 μm; circles, L = 70 μm.

As detailed more completely in our optical-mask experiment (and also in reference [13]), this field dependence can be explained on the basis of the SWAP model; as intimated earlier, at the lower fields the drift velocities are dominated by a field dependent trap-release rate. (Specifically, we have found an inverse relationship between the applied field and the trap-release times following the theoretical framework for one-dimensional trap escape put forward by Wilson [18].) As the field is increased, these trap-release times become smaller and so the observed trap-limited drift velocity of the carriers will incline asymptotically towards their intrinsic field-independent SWAP velocity. This gives rise, then, to the tendency towards saturation found in figure 13. However, despite our premise that the on-chain motion may be that of the SWAP, the actual observed trap-limited mobility as opposed to its possible ultra-high intrinsic

mobility, is small, with a low-field value deduced to be about 8.9×10^{-4} m^2 s^{-1} V^{-1} which is in good agreement with the optical-mask experiments.

Figure 13 also demonstrates a linear scaling between L and t_τ. Again, this is in agreement with results obtained using the optical-mask experiment and shows that, for the applied fields used here, carrier propagation is Gaussian and not dispersive (in the Scher and Montroll sense found in disordered three-dimensional solids [19]). If it were, an anomolous transit time with length dependence would be expected which, as shown by Movaghar *et al* [20] for one-dimensional systems, is given by:

$$t_\tau \propto FL^{\frac{1}{(1-\alpha)}} \tag{4}$$

where α is a disorder parameter and less than unity. Specifically for PDATS, α has been measured to be 0.85 [20], implying therefore that:

$$t_\tau \propto FL^{6.66} \tag{5}$$

which clearly is a relation not observed here.

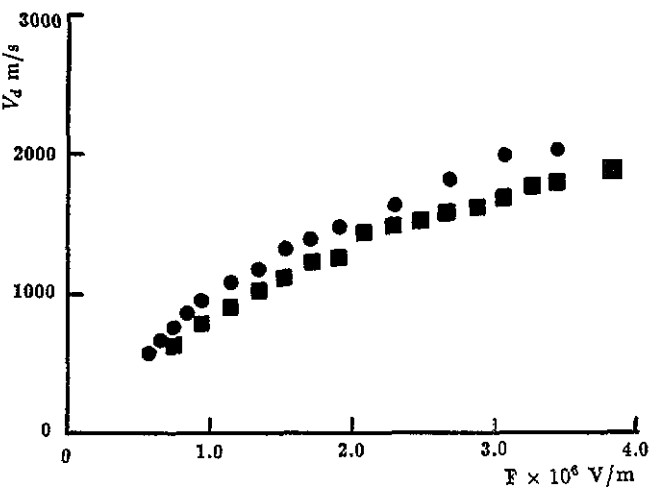

Figure 14. Comparison of field dependence of drift velocity data obtained using the optical mask (circles) with that obtained using the EAD (squares) for the same sample with $D = 520\mu$m.

Finally, figures 14 and 15 are two direct comparisons of the field dependence of drift-velocity results obtained utilizing the EAD with that obtained utilizing the optical mask, using two samples of inter-electrode spacings 520 μm and 300 μm respectively. It is clear that agreement between the two techniques is good and indicates that the possible Coulomb effects hypothesized by Donovan and Wilson as being responsible for the prolific trapping and trap-release events observed in the optical-mask experiments are small. These traps, therefore, must be intrinsic to the sample independent of whether low-density bipolar currents are used or the higher-density unipolar currents.

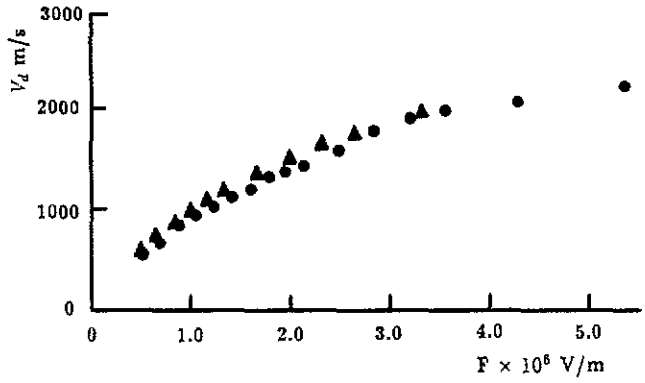

Figure 15. Comparison of field dependence of drift velocity data obtained using the optical mask (circles) with that obtained using the EAD (triangles) for the same sample with $D = 300\ \mu m$.

4. Conclusions

A qualitative explanation for the action of the EAD is given, although there is obvious scope for more theoretical and experimental investigation. (For instance, it would be desirable to have the width of the wire as small as possible with respect to the surface electrode spacing, so that any perturbations of the field lines in the vicinity of the wire are then also small compared to the overall field distribution between the electrodes.) Nevertheless, both the optical-mask experiments and those of the EAD show good agreement with each other. Namely: more dispersive current profiles as the applied field is lowered, the linear scaling of t_τ and L, the similarity of the field dependence of drift velocity plots, and the premise that the electrons are the dominant current carriers.

Their main conclusions of trap-limited transport down to small distances (in the case of the EAD, shown to be much less than 70 μm) and observed mobilities of the order 10^{-4} m^2 s^{-1} V^{-1} are also consistant with the conclusions of Bassler *et al* and Heeger *et al* (This can be clearly seen from figure 16 which shows the field dependence of drift velocity as found by Heeger *et al* plotted onto the data of figure 13.) and, in the author's opinion, cannot be reconciled with the 1 mm inter-trap separations and ultra-high mobilities claimed by Donovan and Wilson. However, both experiments show a drift velocity that tends to saturate at acoustic velocities with high field. This, then, lends itself to the idea of the intrinsic inter-trap drift velocity of the carrier being field saturated as postulated by Wilson [5].

The possible advantage that the EAD has over the optical-mask experiment is its relative simplicity of construction. More sophisticated photographic techniques coupled with much faster laser pulses, should allow access to time-of-flight signals on a much smaller time scale, (and perhaps not just on PDATS). It may then be possible to observe the intrinsic inter-trap SWAP motion. In addition, because carrier densities are in general smaller than those used in the optical-mask experiment, the problem of space charge effects [15,21–23] by the carriers themselves in disturbing the internal applied fields, is significantly reduced. The only restriction on carrier density when using the EAD is the possibility of bimolecular recombination dominating, which then leads to current loss. However for this to occur, laser intensities need to be considerably higher (a factor of at least 100) than those used here [13].

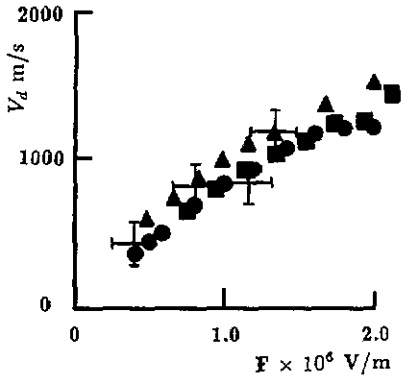

Figure 16. Data from [8] (crosses) plotted with data from figure 13.

Acknowledgments

I thank both Dr D J Willock (University College London (UK)) and Profesor D N Batchelder (Leeds University (UK)) for many useful discussions during the course of this work. I am also grateful to Dr B J E Smith for the excellent quality PDATS crystals. The experiments presented here were conducted at Queen Mary and Westfield College, London. This work has been supported by SERC (UK).

References

[1] Wegner G 1969 *Z. Naturf.* B **24** 824
[2] Pope M and Swenberg C E 1982 *Electronic Processes in Organic Crystals (Monographs on Physics and Chemistry of Materials No 39)* (Oxford: Oxford Science Publications)
[3] Siddiqui A S and Wilson E G 1979 *J. Phys. C: Solid State Phys.* **12** 4237
[4] Donovan K J and Wilson E G 1981 *Phil. Mag.* B **44** 9
[5] Wilson E G 1983 *J. Phys. C: Solid State Phys.* **16** 6739
[6] Donovan K J and Wilson E G 1985 *J. Phys. C: Solid State Phys.* **18** L51
[7] Moses D, Sinclair M and Heeger A J 1987 *Phys. Rev. Lett.* **58** 2710
[8] Moses D and Heeger A J 1989 *J. Phys.: Condens. Matter* **1** 7395
[9] Blum T and Bassler H 1988 *J. Chem. Phys.* **123** 431
[10] Donovan K J and Wilson E G 1990 *J. Phys.: Condens. Matter* **2** 1659
[11] Donovan K J, Elkins J W P and Wilson E G 1991 *J. Phys.: Condens. Matter* **3** 2075
[12] Fisher N E and Willock D J 1992 *J. Phys.: Condens. Matter* submitted
[13] Fisher N E 1990 *PhD Thesis* University of London
[14] Kepler R G 1960 *Phys. Rev.* **119** 1226
[15] LeBlanc O H Jr 1960 *J. Chem. Phys.* **33** 626
[16] Donovan K J, Fisher N E and Wilson E G 1989 *Synth. Met.* **28** D557
[17] Wilson E G 1991 *J. Phys.: Condens. Matter* submitted
[18] Wilson E G 1979 *J. Phys. C: Solid State Phys.* **13** 2885
[19] Scher H and Montroll E W 1975 *Phys. Rev.* B **12** 2455
[20] Movaghar B, Murray D W, Donovan K J and Wilson E G 1984 *J. Phys. C: Solid State Phys.* **17** 1247
[21] Many A, Weisz S Z and Simhony M 1962 *Phys. Rev.* **126** 1989
[22] Many A and Rakavy G 1962 *Phys. Rev.* **126** 1980
[23] Schwartz L M and Hornig J E 1965 *J. Phys. Chem. Solids* **26** 1821